$Na_5Co_{15.5}Te_6O_{36}$: An $S = \frac{1}{2}$ stacked Ising kagome antiferromagnet with a partially disordered ground state

Z. Y. Zhao [1,*] X. Y. Yue,[2] J. Y. Li,[1] N. Li,[3] H. L. Che,[3] X. F. Sun,[2,3] and Z. Z. He [1]

[1]*State Key Laboratory of Structural Chemistry, Fujian Institute of Research on the Structure of Matter, Chinese Academy of Sciences, Fuzhou, Fujian 350002, People's Republic of China*

[2]*Institute of Physical Science and Information Technology, Anhui University, Hefei, Anhui 230601, People's Republic of China*

[3]*Department of Physics, Hefei National Laboratory for Physical Sciences at Microscale, and Key Laboratory of Strongly-Coupled Quantum Matter Physics (CAS), University of Science and Technology of China, Hefei, Anhui 230026, People's Republic of China*

(Received 7 December 2021; accepted 29 March 2022; published 7 April 2022)

$S = \frac{1}{2}$ Ising kagome antiferromagnets (KAFs) are rare in reality. In this paper, we report the magnetic ground state and field-induced transitions of an $S = \frac{1}{2}$ Ising antiferromagnet with a stacked kagome geometry, $Na_5Co_{15.5}Te_6O_{36}$. Upon cooling, magnetic susceptibility measurements reveal three successive magnetic transitions at $T_1 = 45.2$ K, $T_2 = 35.4$ K, and $T_3 \sim 20$ K. When the magnetic field is applied along the Ising c axis, a strikingly anomalous initial magnetization lying outside the hysteresis loop is observed below T_3. Through detailed characterizations, the magnetic field vs temperature phase diagram is established. A partially disordered antiferromagnetic state is proposed below T_1, which becomes frozen below T_3. $Na_5Co_{15.5}Te_6O_{36}$ is therefore a promising candidate for $S = \frac{1}{2}$ Ising KAFs, and this unique composite structure may shed light on the exploratory path for $S = \frac{1}{2}$ Ising KAFs.

DOI: 10.1103/PhysRevB.105.144406

I. INTRODUCTION

The geometry of corner-sharing triangles that impedes the magnetic order renders the $S = \frac{1}{2}$ kagome antiferromagnets (KAFs) a recognized cornerstone to cognize exotic quantum phenomena [1–6]. For Heisenberg spins on a structurally perfect kagome lattice, the degenerate manifold ground states prohibit the magnetic order at 0 K [7]. The $S = \frac{1}{2}$ Heisenberg KAF is therefore an excellent motif for realizing the fascinating quantum spin liquid (QSL), a long-range entangled state of matter hosting emergent gauge fields and fractionalized excitations [4,6,8]. A number of compounds are discovered to be QSL candidates, including the celebrated herbertsmithite $ZnCu_3(OH)_6Cl_2$ [9] and its relatives [10–14], as well as the variant breathing KAF based on V^{4+} (d^1, $S = \frac{1}{2}$) ions [15–17]. On the other hand, for Ising KAFs, the highly frustrated spins can also give rise to various types of magnetic order [18–20]. However, as far as we know, layered $S = \frac{1}{2}$ Ising KAFs have been scarcely found in reality, and the rare candidates hinder the exploration of novel phenomena and relevant physics.

The $S = \frac{1}{2}$ Ising chain, frequently observed in cobalt oxides due to the Kramers nature of Co ions, is also an attractive system and has been reported to show a variety of novel physics, for instance, quantum criticality [21,22], topological excitations [23], Bethe strings [24], and excited bound states with emergent E_8 symmetry [25], etc. It has been found that a composite geometry consisting of Ising chains in a two-dimensional array can inherit the excellent traits of both geometries. For example, in the $S = \frac{1}{2}$ stacked Ising triangular lattice antiferromagnets (TAFs) $ACoX_3$ (A = Rb, Cs; X = Cl, Br) and $Ca_3Co_2O_6$, in which Ising Co chains are arranged in a triangular lattice, not only the domain-wall excitations of the one-dimensional antiferromagnetic (AFM) Ising chain [26,27] but also the magnetization plateau and partially disordered state in the triangular lattice [28–31] are observed. Besides, a disordered ground state is also found in $Ba_3Co_2O_6(CO_3)_{0.7}$ due to its honeycomb structure [32,33]. Inspired by this, placing $S = \frac{1}{2}$ Ising chains in a kagome geometry is an alternative approach to realize $S = \frac{1}{2}$ Ising KAFs; these are named stacked Ising KAFs. In addition, such a composite structure also offers a platform for chemists to search for potential $S = \frac{1}{2}$ Ising KAF candidates and uncover diverse physics.

$Na_5Co_{15.5}Te_6O_{36}$ (NCTO) crystallizes in a hexagonal structure with space group $P6_3/m$ [34,35]. As illustrated in Figs. 1(a)–1(c), there are three crystallographic Co positions which are confirmed to be divalent by Co K-edge x-ray absorption spectroscopy measurements [34]. Thereinto, the edge-shared $Co(1)O_6$ octahedra build zigzag chains along the c direction and are further connected to a kagome lattice in the ab plane, whereas $Co(2)O_6$ and $Co(3)O_6$ trigonal prisms form face-shared chains in an alternate manner and sit in the center of each triangle. It is notable that the Co3 sites are partially occupied by Na atoms, giving rise to an on-site disorder. In view of the Ising anisotropy [35], the topology of Co1 ions can be regarded as a stacked kagome lattice [see Fig. 1(d)], and NCTO is an example of an $S = \frac{1}{2}$ stacked Ising KAF. In this paper, we successfully grow NCTO single crystals and in detail study the magnetic ground state and peculiar field-induced transitions. Three successive magnetic transitions are detected at $T_1 = 45.2$ K, $T_2 = 35.4$ K, and $T_3 \sim 20$ K, respectively. When the magnetic field is applied along

*zhiyingzhao@fjirsm.ac.cn

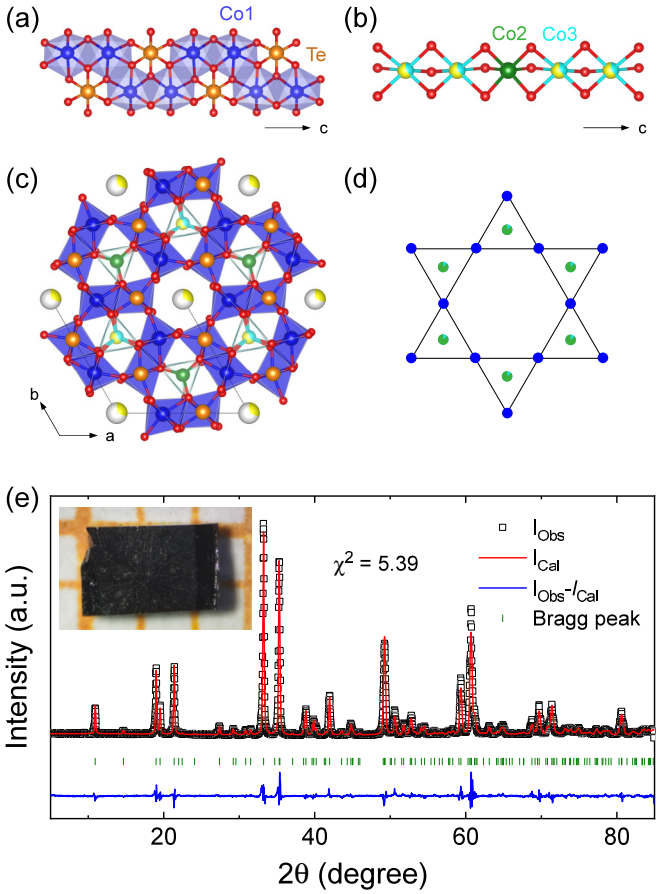

FIG. 1. Crystal structure of NCTO. (a) Zigzag chain of Co1 atoms. (b) Alternate arrangement of Co2 and Co3 atoms. Each Co3 site is partially occupied by a Na atom. (c) Crystal structure projected in the *ab* plane. Na atoms (yellow) sit in the hexagonal channels. The solid frame denotes the unit cell. (d) Topological spin lattice in the *ab* plane. Co1 chains (blue symbols) build a perfect stacked kagome lattice, and Co2-Co3 chains (green-cyan symbols) locate in the center of each triangle. (e) Refinement of the powder x-ray diffraction pattern at room temperature. The inset is a photograph of an NCTO single crystal.

the Ising c axis, a strikingly anomalous initial magnetization is unveiled below T_3. These exceptional phenomena indicate a possible partially disordered antiferromagnetic (PDA) state below T_1 and a frozen PDA state below T_3.

II. EXPERIMENTS

NCTO single crystals were synthesized using a self-flux method. Na_2CO_3, Co_3O_4, and TeO_2 were used as starting materials with a molar ratio of 3 : 2.33 : 6. The mixture was ground thoroughly with alcohol and placed in an alumina crucible. The growth ampoule was then heated to 1000 °C in 10 h, kept for 2 days, and slowly cooled to 600 °C with a rate of 2 °C/h. After that, the furnace was cooled to room temperature in 7 h. The as-grown single crystals shown in Fig. 1(e) are dark purple with the growth direction parallel to the c axis. The phase purity was checked by the powder x-ray diffraction; see Fig. 1(e).

The dc magnetic susceptibility was measured using one piece of crystal with mass of 21.7 mg between 2 and 300 K by using a superconducting quantum interference device vibrating sample magnetometer (SQUID-VSM; Quantum Design). The ac magnetic susceptibility measurements were performed using the same piece of crystal on the SQUID-VSM (Quantum Design) with applied frequencies between 15 and 1000 Hz in the temperature range from 2 to 60 K. Heat capacity measurements were carried out on another piece of crystal about 9 mg using the relaxation method in the temperature range from 2 to 200 K on a physical property measurement system (PPMS; Quantum Design).

III. RESULTS AND DISCUSSION

A. Magnetic anisotropy

Figure 2(a) shows the temperature dependencies of the magnetic susceptibility with applied magnetic fields parallel ($\chi_\parallel$) and perpendicular ($\chi_\perp$) to the crystallographic c direction. The large difference between $\chi_\parallel$ and $\chi_\perp$ reflects a strong Ising anisotropy with the easy axis along the c direction. Upon cooling, $\chi_\parallel$ undergoes two successive AFM transitions, which are identified by the rapid drop at $T_1 = 45.2$ K and a shoulderlike anomaly at $T_2 = 35.4$ K. Both transitions are determined as the peak positions from the differential curve. With further lowering of the temperature, a bifurcation between field-cooling (FC) and zero-field-cooling (ZFC) branches is observed below $T_3 \sim 20$ K; see Fig. 2(b). Besides, a rather weak frequency dependence of ac susceptibility χ' is also found in Fig. 2(c). In contrast, $\chi_\perp$ is monotonously increased with decreasing temperature and exhibits a very weak anomaly only around T_1. No ZFC-FC splitting is found in $\chi_\perp$. The high-temperature magnetic susceptibility behaves in a Curie-Weiss manner and gives the Weiss temperatures $\theta_{CW}^{\parallel} = 13.1(9)$ K and $\theta_{CW}^{\perp} = -21.1(2)$ K. The anisotropic Weiss temperature with a sign change suggests that the Curie-Weiss behavior primarily originates from the single-ion anisotropy [33,36–41]. From the crystal structure, the ∠Co1-O-Co1 within the zigzag chain is between 84.7° and 96.1°, which favors a ferromagnetic (FM) intrachain coupling according to the Goodenough-Kanamori rule [42]. The fast increase in $\chi_\parallel$ below 150 K is thus ascribed to the development of short-range FM correlation. Correspondingly, the transition at T_1 is associated with the AFM order of ferromagnetically coupled Co1 chains.

The isothermal magnetizations parallel ($M_\parallel$) and perpendicular ($M_\perp$) to the c direction in Fig. 2(d) are distinct, confirming the strong single-axis anisotropy. The moment at 7 T is about 1.6 μ_B, consistent with the previous work [35]. The reduced moment of Co^{2+} ions suggests an effective $S = \frac{1}{2}$ under the cooperative effect of spin-orbit coupling and the crystal-field effect. The most remarkable feature is the presence of a large hysteresis loop in $M_\parallel$ up to 7 T. In view of the on-site disorder between Co3 and Na ions, the magnetic inhomogeneity is intuitively responsible for the observed ZFC-FC bifurcation in $\chi_\parallel$ and the frequency-dependent χ'. However, this is not compatible with the pronounced magnetization hysteresis, ruling out the possibility of a glassy ground state. Considering the high fraction of Co1 ions (~80%) in NCTO,

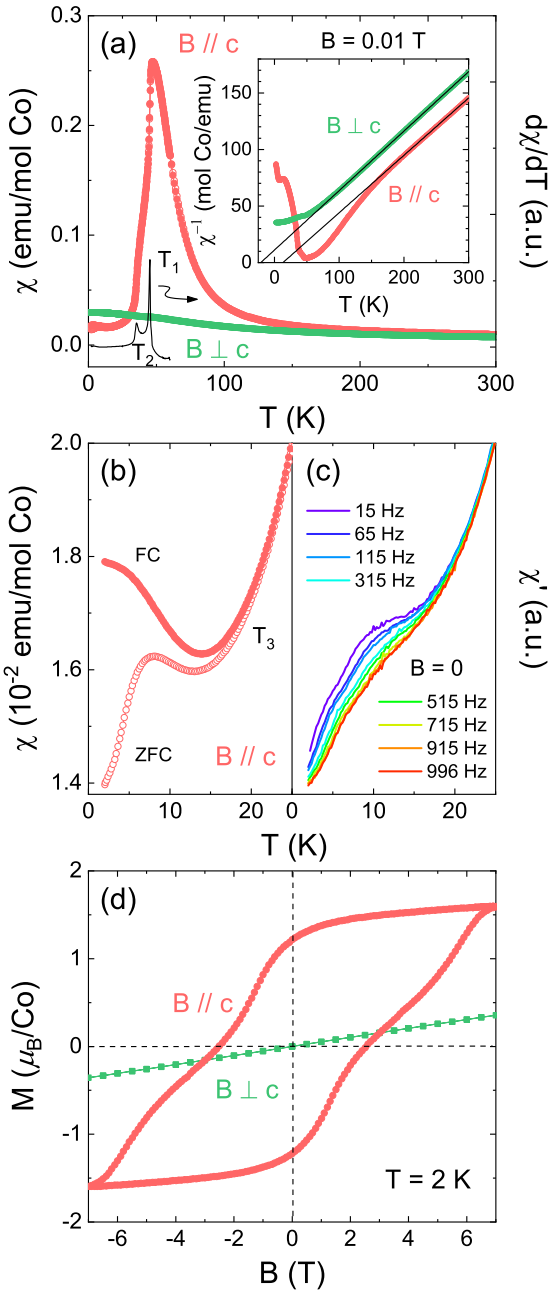

FIG. 2. Anisotropic magnetic properties of NCTO. (a) Temperature dependencies of dc magnetic susceptibility $\chi_{\parallel}$ and $\chi_{\perp}$ for both field-cooling (FC, solid symbols) and zero-field-cooling (ZFC, open symbols) measurements in 0.01 T. The differential curve for $\chi_{\parallel}$ is also plotted to define the transition temperature T_1 and T_2. The inset shows the reciprocals of $\chi_{\parallel}$ and $\chi_{\perp}$ measured after ZFC. Solid lines are the Curie-Weiss fittings. (b) A magnified view of $\chi_{\parallel}$ below 25 K. (c) ac susceptibility measured at different frequencies without an external magnetic field. The applied oscillation field is 2 Oe. (d) Magnetization $M_{\parallel}$ and $M_{\perp}$ at 2 K.

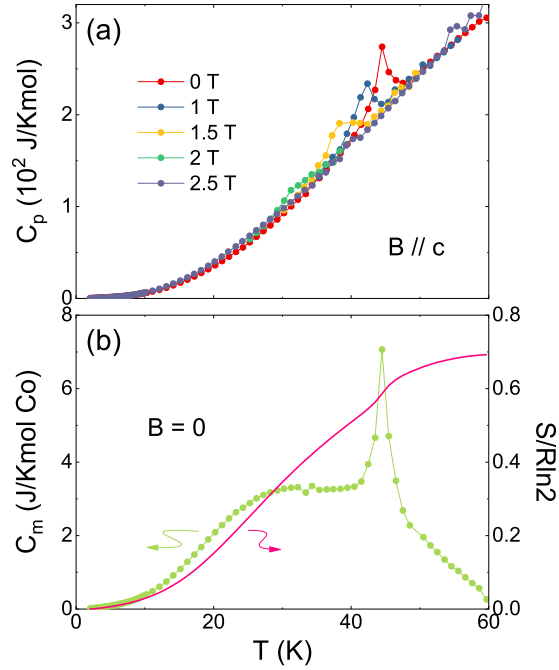

FIG. 3. (a) Specific heat measured in magnetic fields along the c axis up to 2.5 T. (b) Magnetic specific heat and estimated entropy recovery in zero field.

the significant irreversible magnetization, which disappears above T_3 in Fig. S1 of the Supplemental Material [43], is probably predominant from the Co1 sublattice. The weak transition at T_2, however, is probably related to the AFM order of Co2-Co3 chains. This implies some weak but non-negligible interactions between adjacent Co1 and Co2-Co3 chains.

B. Magnetic transitions for $B \parallel c$

Considering the Ising anisotropy of Co^{2+} ions, below we will focus on the investigation of magnetic properties under the application of a magnetic field along the c direction.

First, the specific heat C_p measured in various magnetic fields is shown in Fig. 3(a). It is of great interest to see that the zero-field C_p only displays one sharp λ peak at T_1. At lower temperatures, C_p is smoothly decreased, and there is no anomaly associated with the transition at T_2 or T_3. With increasing field, T_1 is gradually reduced and vanishes above $B^* = 2.5$ T (Fig. S2). The temperature dependence of the zero-field C_p above 60 K can be reproduced using the Einstein model [44] (Fig. S3) and gives two Einstein temperatures, $\Theta_{E1} = 199.3(6)$ K and $\Theta_{E2} = 666(1)$ K. The magnetic specific heat is then extracted after subtracting the lattice contribution, and the magnetic entropy is calculated to be $0.7R\ln 2$, which is a little smaller than the expectation for $S = \frac{1}{2}$ systems, as shown in Fig. 3(b).

Figure 4(a) presents the temperature dependencies of $\chi_{\parallel}$ measured in various magnetic fields after ZFC. Although T_1 and T_2 are monotonously reduced with increasing field, $\chi_{\parallel}$ exhibits a distinct tendency in low and high fields, as shown in Figs. 4(b) and 4(c). On the one hand, T_1 is gradually reduced from 45.2 K in 0.1 T to 30 K in 2 T and rapidly decreased to 12.6 K in 2.5 T; in higher fields, T_1 is further reduced slowly again. On the other hand, $d\chi/dT$ at T_1 is firstly suppressed up to 2 T and then becomes enhanced again above B^*. Similarly, the feature at T_2 is firstly weakened with increasing field and is nearly invisible in 1.5 T; above 2 T, another transition defined

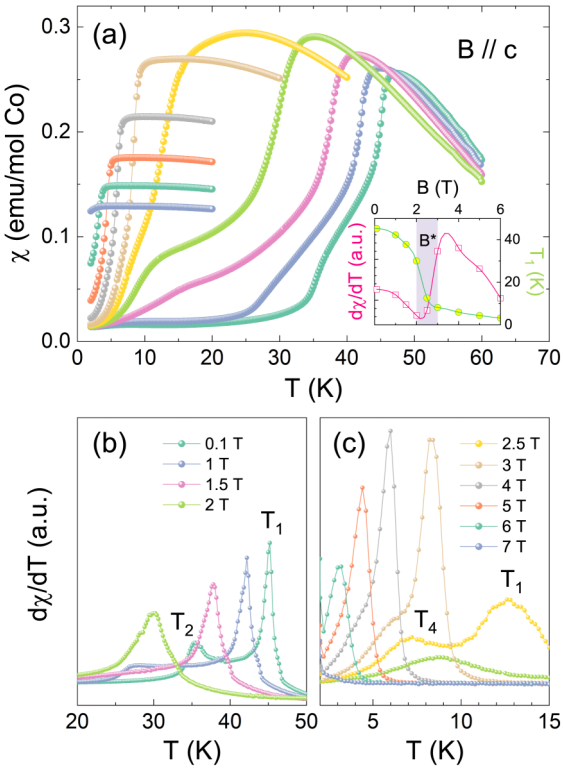

FIG. 4. (a) Temperature dependencies of the dc susceptibility measured in various fields after ZFC. The curve measured in 0.01 T, which is almost identical to the 0.1-T one, is omitted for clarity. The inset shows the field dependencies of T_1 and the corresponding magnitude of the differential at T_1. B^* is the critical field determined from the specific heat measurements. (b) and (c) The corresponding differential curves.

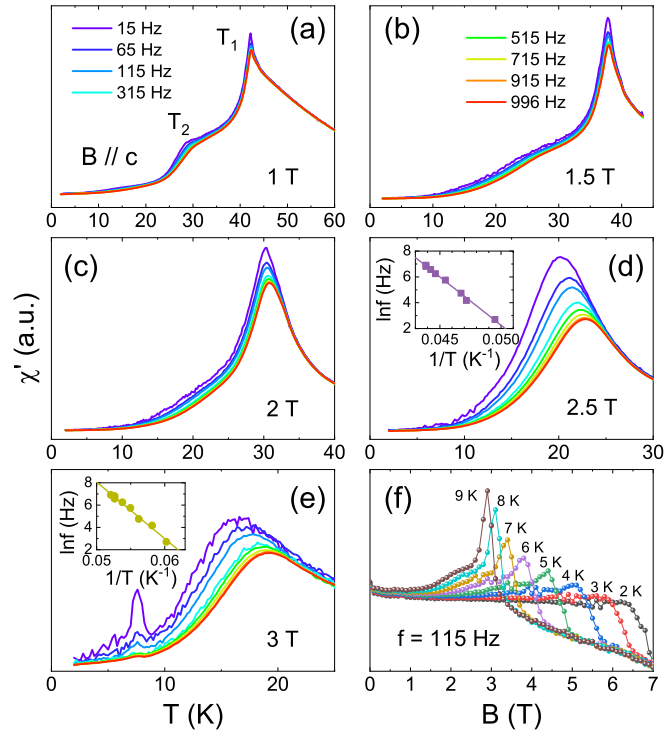

FIG. 5. (a)–(e) Temperature dependencies of the ac susceptibility measured with an oscillating field of 2 Oe. The insets in (d) and (e) are the fittings according to the Arrhenius law. (f) Field dependencies of the ac susceptibility measured at different temperatures with $f =$ 115 Hz.

as T_4 appears and becomes strengthened above B^*. As the field is increased further, the two transitions at T_1 and T_4 move closer and finally merge together in 4 T. In higher fields, this transition is continuously suppressed with a quickly weakened magnitude. The field dependencies of T_1 and the corresponding $d\chi/dT$ magnitude [inset in Fig. 4(a)] indicate a clear anomaly around B^*, a critical field that completely suppresses the λ peak in C_p. It is noteworthy that in contrast to the specific heat result, T_1 is persistent up to 6 T in $\chi_\parallel$.

The ac susceptibility χ' as a function of temperature is carried out to further trace the magnetic transitions. In the absence of an external magnetic field, as shown in Figs. 2(c) and S4, χ' is independent of the frequency at T_1 and T_2, but a rather weak frequency dependence is found below T_3. As displayed in Figs. 5(a)–5(e), the transition at T_2 in 1 T also becomes frequency dependent, but T_1 is still robust except for a slightly reduced magnitude. The T_1 peak starts to show weak relaxation in 1.5 T which becomes obvious in 2 T. Meanwhile, the T_2 and T_3 transitions are too broad to distinguish. In $B^* =$ 2.5 T, a strong frequency-dependent peak is emergent around 20 K, and the T_1 transition (12.6 K for $\chi_\parallel$ in 2.5 T) vanishes. According to the Arrhenius law, the derived energy barrier is about 748 K. This feature moves to lower temperatures in 3 T, and the energy barrier is decreased to 507 K. In 3 T, the T_1 transition (8.2 K for $\chi_\parallel$) reappears again as evidenced by the presence of a weak anomaly. In higher fields, T_1 is further reduced though χ' is more noisy (Fig. S5).

The virgin magnetization measured at various temperatures is plotted in Fig. 6. At 2 K, two magnetic transitions are detected at $B_1 = 4.9$ T and $B_2 = 6.5$ T, as determined from the differential curve in Fig. 6(b). Upon warming, both B_1 and B_2 are decreased with a gradual enhancement of the dM/dB magnitude below 10 K. However, the dM/dB magnitude at B_2 keeps stable up to 20 K and then weakens at higher temperatures. In the meantime, the dM/dB magnitude at B_1 which is evidenced as a small sharp peak at lower temperatures evolves into a broad shoulder above 15 K. Here, we define B_3 as the critical field where the shoulder feature emerges. At 30 K, B_3 is about 0.9 T and becomes invisible at higher temperatures; B_2 is suppressed to 1.3 T at 40 K (Fig. S6). At 2 K, the magnetic entropy change in 7 T is calculated to be about 4.3 J/Kmol per Co, consistent with the specific heat result (Fig. S7).

C. Anomalous hysteresis loop

When the field is applied along the c axis, the magnetization presents a pronounced history dependence, and several interesting features are observed in Fig. 7. First, the virgin curve (path 1), which is recorded with ascending field from 0 to 7 T after cooling from the paramagnetic state in zero field, lies outside the hysteresis loop in higher fields. This is very different from conventional ferromagnets, in which the virgin curve locates within the loop due to the multiple-domain

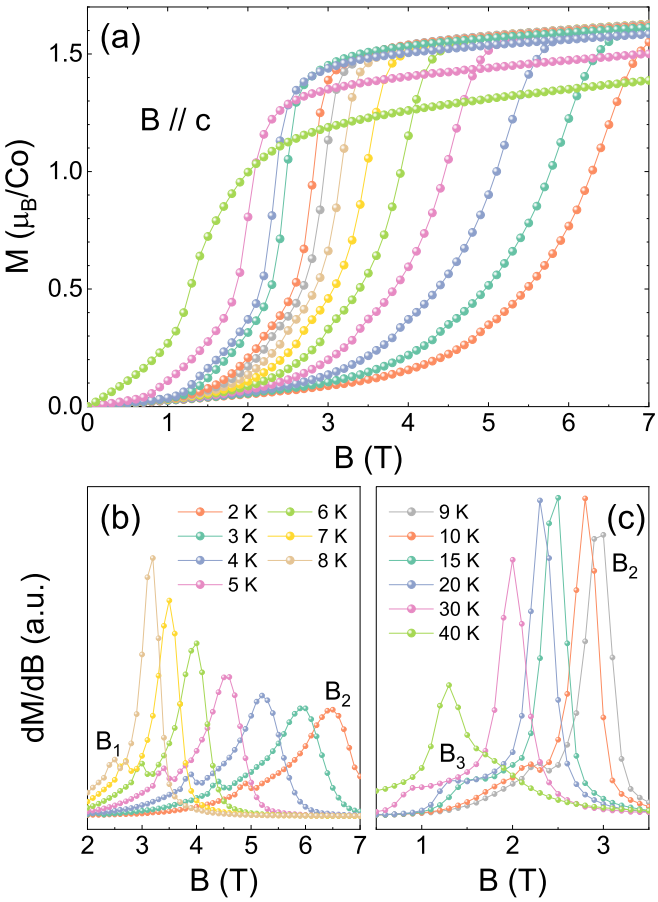

FIG. 6. (a) Field dependencies of the initial magnetization in $M_{\|}$ measured at several constant temperatures after ZFC. (b) and (c) Differential curves below 8 K and above 9 K, respectively.

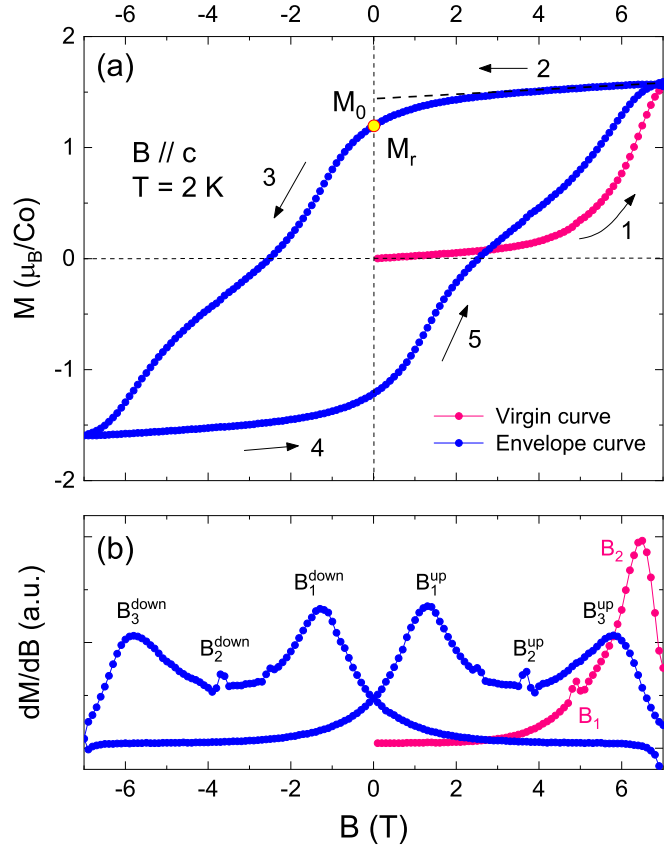

FIG. 7. Magnetization of NCTO for $B \parallel c$ at $T = 2$ K. (a) Magnetization hysteresis loop. The virgin curve is measured from 0 to 7 T after ZFC, followed by a complete field excursion (7 T $\rightarrow$ -7 T $\rightarrow$ 7 T). The numbered arrows denote the history of the field sweeping. The dashed line is a linear extrapolation from high fields with an intercept M_0. The remanent magnetization M_r is represented by the yellow dot. (b) Corresponding differential curves. Multiple magnetic transitions are labeled by the critical fields.

effect. Second, the nearly linear increase of the moment in the low-field virgin curve is as expected for antiferromagnets. With further increasing field, two magnetic transitions are detected at B_1 and B_2. Third, when the field is released to zero (path 2), the disappearance of the magnetic transitions can be interpreted in terms of the domain reorientation in ferromagnets. Fourth, when the field is reversed (path 3), three successive magnetic transitions emerge at $B_1^{\text{down}} = -1.3$ T, $B_2^{\text{down}} = -3.7$ T, and $B_3^{\text{down}} = -5.8$ T [the weak anomaly at -2.5 T in Fig. 7(b) is due to the sign change of the magnetization]. Fifth, in the second field-up process (path 5), the successive magnetic transitions appear again at B_1^{up} ($= -B_1^{\text{down}}$), B_2^{up} ($= -B_2^{\text{down}}$), and B_3^{up} ($= -B_3^{\text{down}}$). It should be mentioned that the critical fields B_2^{up} and B_3^{up} in the subsequent field excursion are a bit lower than B_1 and B_2 in the virgin curve. Since the anomalous initial magnetization along with the higher critical fields is persistent up to T_3 (Fig. S1), a common origin should be in charge of both features.

This exceptional magnetization with concurrence of the large hysteresis loop and anomalous virgin curve is rarely observed in magnets. Two mechanisms from the literature, the metastable ground state and the kinetic arrest of a first-order AFM-FM transition, may result in similar magnetization behavior. However, after careful comparisons with our experimental results, both mechanisms are considered to be not responsible for the anomalous magnetization hysteresis in NCTO. The reasons are the following.

(i) After cooling in zero field, a metastable ground state could be developed due to the disordered domain walls. It has been reported in the orthoferrite $DyFeO_3$ that the virgin magnetization curve shows two successive spin orientations below 2 K but only the higher-field one is kept in the following field excursion, giving rise to an irreversible initial magnetization [45]. Similar behavior is also observed in the field dependence of the capacitance in the orthoferrite $TbFeO_3$ [46]. However, in both orthoferrites no large hysteresis loop is developed, in contrast to the significant hysteresis feature in NCTO. Besides, in the Y-type hexaferrite $Ba_{2-y}Sr_yCo_2Fe_{12-x}Al_xO_{22}$ ($x = 0.9$), the initial magnetization is located outside the loop with a much lower magnitude, but the critical field is unchanged when the field is reversed [47]. This also disagrees with our results for NCTO, which show higher critical fields in the virgin curve.

(ii) The kinetics of a first-order transition, governed by the time required to extract the latent heat of the system, can be arrested by rapid change in the environment. In some intermetallic alloys [48–51], the system has an AFM ground state

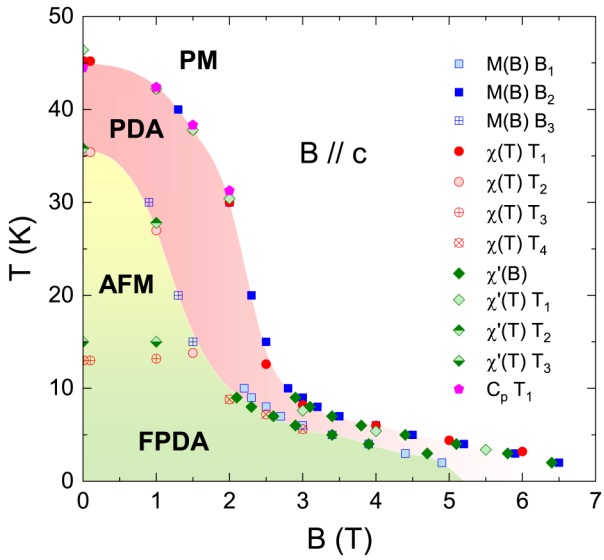

FIG. 8. Magnetic field vs temperature phase diagram of NCTO for $B \parallel c$. The data are extracted from the ZFC measurements through various experiments. PM, AFM, PDA, and FPDA, paramagnetic phase, antiferromagnetic phase, partially disordered antiferromagnetic phase, and frozen partially disordered antiferromagnetic phase, respectively.

and undergoes a field-induced AFM-FM transition. As the field is released, the kinetics of the FM-AFM transition is hindered with a fraction of the frozen FM regime. The resultant state in zero field is thus a coexisting stable AFM phase along with the kinetically arrested metastable FM phase. When the field is ramped up again, the magnetization then starts from this coexistent state rather than the original AFM state as in the virgin curve. The forward magnetization is thus larger than the initial magnetization due to the larger moment of the FM phase, leaving the virgin curve lying below the hysteresis envelope. The kinetic arrest is always accompanied with a first-order transition, which is also contradictory to NCTO showing two second-order magnetic transitions at B_1 and B_2.

D. Phase diagram

Based on the above experimental results, the magnetic field vs temperature phase diagram for NCTO is illustrated in Fig. 8. As mentioned above, the transitions at T_1 and T_3 are probably associated with the Co1 sublattice, while the transition at T_2 is likely related to Co2-Co3 chains. The observed experimental phenomena below T_3, including the FC-ZFC bifurcation in $\chi_\parallel$, the spin-dynamic behavior in χ', and the pronounced magnetization hysteresis in $M_\parallel$, are reminiscent of the stacked TAFs $A_3BB'O_6$ (A = Ca, Sr; B = Co, Ni; B' = Co, Rh, Ir). In this family, with descending temperature, the magnetic sublattice firstly develops a PDA state, in which two-thirds of the magnetically ordered chains align in opposite orientations and the remaining one-third of the chains remain incoherent with each other and keep fluctuating. At lower temperatures, the chains belonging to this incoherent one-third freeze randomly [frozen PDA (FPDA) state], resulting in a large ZFC-FC splitting in the magnetic susceptibility and a significant magnetization hysteresis; in addition, a slow spin relaxation behavior is uncovered by the ac susceptibility measurements [52–55]. Nevertheless, it is noteworthy that in NCTO the specific heat shows a weak λ anomaly at T_1 with 70% entropy recovery. This is different from $A_3BB'O_6$, in which no signature associated with the PDA state is realized across the transition [53,55–57], but similar to another stacked Ising TAF, $CsCoBr_3$, with a λ peak across the PDA state [30,58]. Recently, an organic compound, $CoCl_2$-2SC$(NH_2)_2$, with a triangular lattice is also reported to show a PDA ground state, in which the λ anomaly is clearly observed in C_p with only 40% expected entropy [38].

For these reasons, the Co1 sublattice in NCTO is proposed to undergo a PDA state below T_1 and enter into a FPDA state below T_3. The transition at T_2 is then associated with the AFM order of Co2-Co3 chains. It should be mentioned that a recent paper involving neutron powder diffraction (NPD) measurements has proposed a canted AFM structure with a $\mathbf{k} = (0.5\ 0.5\ 0)$ propagation vector [34], in which all the Co1 FM chains are arranged in a ferrimagnetic configuration on a basal triangle. However, the simple analysis of the NPD pattern at low temperatures is not informative enough to elucidate the nature of the magnetic order. As discussed in Ca_3CoRhO_6, both PDA and ferrimagnetic structures are explained qualitatively from the NPD pattern [59], but the PDA state is later confirmed through the powerful polarized neutron diffraction measurements [60]. To further examine the magnetic ground state and deeply understand the physics, it is necessary to carry out local probes such as neutron scattering, nuclear magnetic resonance, and muon spin relaxation experiments.

E. PDA state in a kagome lattice

The topology of the Co1 sublattice can be viewed as a perfect $S = \frac{1}{2}$ stacked Ising kagome lattice; see Fig. 1(d). Since there are two field-induced magnetic transitions in the virgin curve, the proposed evolution of the spin configurations is sketched in Fig. 9(a). In zero field, two-thirds of the FM coupled Ising chains are antialigned, and the remaining one-third are incoherent FM chains that are frozen with random orientations. As the field is increased, the frozen chains are gradually directed to the field, which is responsible for the initially slow increase in the magnetization. At B_1, all the incoherent FM chains are oriented parallel to the magnetic field. With further increase in the field, the FM chains with spins antiparallel to the field flip, giving rise to the saturated magnetization at B_2.

In addition, the extensive degeneracy of the PDA state can also explain the higher critical fields in the virgin curve, as proposed in Sr_3NiIrO_6 [61]. Considering the coordination number ($z = 4$) for a kagome lattice, each incoherent FM chain should be surrounded by two spin-up chains and two spin-down chains to ensure the cancellation of the AFM interchain interactions. Figure 9(b) illustrates the six possible configurations of the PDA state on a kagome lattice. When including further-neighbor interactions, novel n-sublattice PDA states might come out [62]. Since each incoherent FM chain can be surrounded by multiple configurations of ordered chains, the magnetic field should overcome the stochastic spread of the interchain interaction before the chain flip can be accomplished, which results in the higher critical fields in the

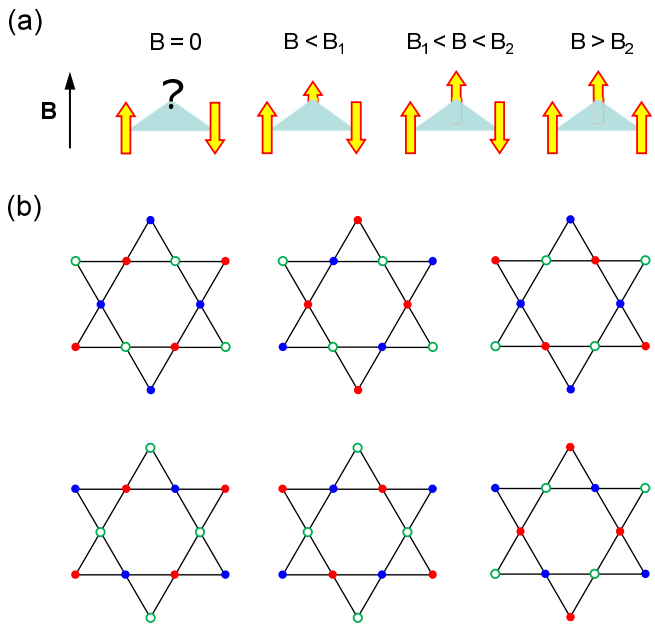

FIG. 9. Proposed spin configurations in NCTO for $B \parallel c$. (a) Evolution of the spin structures of the Co1 sublattice below T_3. The size of the arrow denotes the magnitude of the Co1 moment. (b) Several configurations of the PDA state on a stacked kagome lattice. Green open circles denote the incoherent FM chains, and the red (blue) solid circles denote the FM chains with up (down) spins.

virgin curve. In the subsequent field excursion, the degeneracy is then removed, and the chain flips could be driven by a lower critical field.

From Fig. 8, it is clearly seen that the AFM state of Co2-Co3 chains is enclosed by the PDA and FPDA phases and is easily overcome above B^* due to the rather weak interchain interactions. There is also a critical regime, and several eccentric behaviors are found when the system passes through this area by either sweeping the field around $B^* = 2.5$ T or ramping the temperature near $T^* \sim 15$ K. First, the upper and lower boundaries of the PDA phase change to a much slower slope above B^*. Second, the λ anomaly in C_p is smeared out above B^*. Third, T_1 determined from $\chi_\parallel$ shows a rapid drop around B^*, and meanwhile the $d\chi/dT$ magnitude exhibits a nonmonotonous field dependence. Fourth, the transition at T_1 in χ' disappears around B^* and shows up again in higher fields. In particular, an obvious spin relaxation is observed in the vicinity of the critical field. Fifth, the dM/dB magnitude follows a nonmonotonous temperature dependence near T^*. All these experimental observations imply a crossover behavior once the Co2-Co3 spins are fully polarized, which implies a non-negligible interplay between the Co1 sublattice and Co2-Co3 chains. In higher fields, the boundary between the PDA state and the paramagnetic state becomes indistinguishable. This is confirmed by the field dependence of the ac susceptibility with an applied $f = 115$ Hz, as seen in Fig. 5(f). At 2 K, χ' is nearly field independent in lower fields and exhibits a steplike decrease around 6.4 T. Upon warming, the decrease gradually transforms to a sharp peak with a gradually suppressed critical field. Besides, a weak anomaly located around 4.7 T is also found at 3 K and is developed to a shoulder centered at 2.1 T at 9 K.

IV. CONCLUSIONS

In summary, we perform comprehensive characterizations of the magnetic ground state and field-induced transitions in $Na_5Co_{15.5}Te_6O_{36}$ and construct the magnetic field vs temperature phase diagram. In this compound, zigzag chains formed by the edge-shared $Co(1)O_6$ octahedra are arranged in a perfect kagome geometry, developing a stacked kagome lattice. It is discussed that this peculiar lattice undergoes a PDA state below $T_1 = 45.2$ K and enters into a FPDA state below $T_3 \sim 20$ K. This scenario explains well the pronounced magnetization hysteresis and the exceptional initial magnetization lying outside the hysteresis loop with much higher critical fields. $Na_5Co_{15.5}Te_6O_{36}$ is therefore an example of an $S = \frac{1}{2}$ stacked Ising KAF. This unusual composite geometry opens a brand-new field to search for $S = \frac{1}{2}$ Ising KAFs. Exploration with various Ising chains will promote the progress of novel phenomena and in-depth understanding of the relevant physics.

ACKNOWLEDGMENTS

The work at Fujian Institute of Research on the Structure of Matter, CAS (Z.Y.Z., J.Y.L., and Z.Z.H.), was supported by the National Natural Science Foundation of China (Grants No. 52072368 and No. 21875249). The work at Anhui University (X.Y.Y.) was sponsored by the National Natural Science Foundation of China (Grants No. 12104010 and No. U1832209). The work at University of Science and Technology of China (N.L., H.L.C., and X.F.S.) was financed by the National Natural Science Foundation of China (Grants No. 11874336 and No. U1832209).

[1] R. Moessner and A. P. Ramirez, Phys. Today **59**(2), 24 (2006).
[2] M. R. Norman, Rev. Mod. Phys. **88**, 041002 (2016).
[3] P. Mendels and F. Bert, C. R. Phys. **17**, 455 (2016).
[4] L. Balents, Nature (London) **464**, 199 (2010).
[5] D. S. Inosov, Adv. Phys. **67**, 149 (2019).
[6] Y. Zhou, K. Kanoda, and T. K. Ng, Rev. Mod. Phys. **89**, 025003 (2017).
[7] P. Lecheminant, B. Bernu, C. Lhuillier, L. Pierre, and P. Sindzingre, Phys. Rev. B **56**, 2521 (1997).
[8] L. Savary and L. Balents, Rep. Prog. Phys. **80**, 016502 (2017).
[9] T. H. Han, J. S. Helton, S. Chu, D. G. Nocera, J. A. Rodriguez-Rivera, C. Broholm, and Y. S. Lee, Nature (London) **492**, 406 (2012).
[10] E. Kermarrec, P. Mendels, F. Bert, R. H. Colman, A. S. Wills, P. Strobel, P. Bonville, A. Hillier, and A. Amato, Phys. Rev. B **84**, 100401(R) (2011).
[11] Z. Feng, W. Yi, K. Zhu, Y. Wei, S. Miao, J. Ma, J. Luo, S. Li, Z. Y. Meng, and Y. Shi, Chin. Phys. Lett. **36**, 017502 (2019).
[12] Z. Feng, Z. Li, X. Meng, W. Yi, Y. Wei, J. Zhang, Y. C. Wang, W. Jiang, Z. Liu, S. Li, F. Liu, J. Luo, S. Li, G. Zheng,

Z. Y. Meng, J. W. Mei, and Y. Shi, Chin. Phys. Lett. **34**, 077502 (2017).
[13] B. Fåk, E. Kermarrec, L. Messio, B. Bernu, C. Lhuillier, F. Bert, P. Mendels, B. Koteswararao, F. Bouquet, J. Ollivier, A. D. Hillier, A. Amato, R. H. Colman, and A. S. Wills, Phys. Rev. Lett. **109**, 037208 (2012).
[14] Y. Li, B. Pan, S. Li, W. Tong, L. Ling, Z. Yang, J. Wang, Z. Chen, Z. Wu, and Q. Zhang, New J. Phys. **16**, 093011 (2014).
[15] F. H. Aidoudi, D. W. Aldous, R. J. Goff, A. M. Z. Slawin, J. P. Attfield, R. E. Morris, and P. Lightfoot, Nat. Chem. **3**, 801 (2011).
[16] L. Clark, J. C. Orain, F. Bert, M. A. De Vries, F. H. Aidoudi, R. E. Morris, P. Lightfoot, J. S. Lord, M. T. F. Telling, P. Bonville, J. P. Attfield, P. Mendels, and A. Harrison, Phys. Rev. Lett. **110**, 207208 (2013).
[17] J. C. Orain, B. Bernu, P. Mendels, L. Clark, F. H. Aidoudi, P. Lightfoot, R. E. Morris, and F. Bert, Phys. Rev. Lett. **118**, 237203 (2017).
[18] M. Wolf and K. D. Schotte, J. Phys. A: Math. Gen. **21**, 2195 (1988).
[19] T. Takagi and M. Mekata, J. Phys. Soc. Jpn. **62**, 3943 (1993).
[20] P. Azaria, H. T. Diep, and H. Giacomini, Phys. Rev. Lett. **59**, 1629 (1987).
[21] Y. Cui, H. Zou, N. Xi, Zhangzhen He, Y. X. Yang, L. Shu, G. H. Zhang, Z. Hu, T. Chen, Rong Yu, J. Wu, and W. Yu, Phys. Rev. Lett. **123**, 067203 (2019).
[22] Z. Wang, T. Lorenz, D. I. Gorbunov, P. T. Cong, Y. Kohama, S. Niesen, O. Breunig, J. Engelmayer, A. Herman, J. Wu, K. Kindo, J. Wosnitza, S. Zherlitsyn, and A. Loidl, Phys. Rev. Lett. **120**, 207205 (2018).
[23] Q. Faure, S. Takayoshi, S. Petit, V. Simonet, S. Raymond, L. P. Regnault, M. Boehm, J. S. White, M. Månsson, C. Rüegg, P. Lejay, B. Canals, T. Lorenz, S. C. Furuya, T. Giamarchi, and B. Grenier, Nat. Phys. **14**, 716 (2018).
[24] Z. Wang, J. Wu, W. Yang, A. K. Bera, D. Kamenskyi, A. T. M. N. Islam, S. Xu, J. M. Law, B. Lake, C. Wu, and A. Loidl, Nature (London) **554**, 219 (2018).
[25] R. Coldea, D. A. Tennant, E. M. Wheeler, E. Wawrzynska, D. Prabhakaran, M. Telling, K. Habicht, P. Smeibidl, and K. Kiefer, Science **327**, 177 (2010).
[26] M. Mena, N. Hänni, S. Ward, E. Hirtenlechner, R. Bewley, C. Hubig, U. Schollwöck, B. Normand, K. W. Krämer, D. F. McMorrow, and Ch. Rüegg, Phys. Rev. Lett. **124**, 257201 (2020).
[27] H. B. Braun, J. Kulda, B. Roessli, D. Visser, K. W. Krämer, H. U. Güdel, and P. Böni, Nat. Phys. **1**, 159 (2005).
[28] V. Hardy, M. R. Lees, O. A. Petrenko, D. McK. Paul, D. Flahaut, S. Hébert, and A. Maignan, Phys. Rev. B **70**, 064424 (2004).
[29] N. P. Hänni, D. Sheptyakov, M. Mena, E. Hirtenlechner, L. Keller, U. Stuhr, L. P. Regnault, M. Medarde, A. Cervellino, C. Rüegg, B. Normand, and K. W. Krämer, Phys. Rev. B **103**, 094424 (2021).
[30] J. Wang, D. P. Belanger, and B. D. Gaulin, Phys. Rev. B **49**, 12299 (1994).
[31] Y. Nishiwaki, T. Nakamura, A. Oosawa, K. Kakurai, N. Todoroki, N. Igawa, Y. Ishii, and T. Kato, J. Phys. Soc. Jpn. **77**, 104703 (2008).
[32] H. Igarashi, Y. Shimizu, Y. Kobayashi, and M. Itoh, Phys. Rev. B **89**, 054431 (2014).
[33] K. Boulahya, U. Amador, M. Parras, and J. M. González-Calbet, Chem. Mater. **12**, 966 (2000).
[34] R. A. Saha, J. Sannigrahi, I. Carlomagno, S. Kaushik, C. Meneghini, M. Itoh, V. Siruguri, and S. Ray, arXiv:2107.00262.
[35] Y. J. Shan, Y. Yoshioka, M. Wakeshima, K. Tezuka, and H. Imoto, J. Solid State Chem. **211**, 63 (2014).
[36] D. C. Johnston, Phys. Rev. B **95**, 094421 (2017).
[37] B. K. Rai, A. D. Christianson, D. Mandrus, and A. F. May, Phys. Rev. Materials **3**, 034005 (2019).
[38] E. Mun, F. Weickert, J. Kim, B. L. Scott, C. F. Miclea, R. Movshovich, J. Wilcox, J. Manson, and V. S. Zapf, Phys. Rev. B **93**, 104407 (2016).
[39] P. A. Joy and S. Vasudevan, Phys. Rev. B **46**, 5425 (1992).
[40] J. Q. Yan, S. Okamoto, Y. Wu, Q. Zheng, H. D. Zhou, H. B. Cao, and M. A. McGuire, Phys. Rev. Materials **3**, 074405 (2019).
[41] M. A. McGuire, Q. Zheng, J. Yan, and B. C. Sales, Phys. Rev. B **99**, 214402 (2019).
[42] J. B. Goodenough, *Magnetism and the Chemical Bond* (Interscience, New York, 1963).
[43] See Supplemental Material at http://link.aps.org/supplemental/10.1103/PhysRevB.105.144406 for the detailed magnetization hysteresis, specific heat, and ac susceptibility results.
[44] A. Tari, *Specific Heat of Matter at Low Temperatures* (Imperial College Press, London, 2003).
[45] Z. Y. Zhao, X. Zhao, H. D. Zhou, F. B. Zhang, Q. J. Li, C. Fan, X. F. Sun, and X. G. Li, Phys. Rev. B **89**, 224405 (2014).
[46] S. Artyukhin, M. Mostovoy, N. P. Jensen, D. Le, K. Prokes, V. G. de Paula, H. N. Bordallo, A. Maljuk, S. Landsgesell, H. Ryll, B. Klemke, S. Paeckel, K. Kiefer, K. Lefmann, L. T. Kuhn, and D. N. Argyriou, Nat. Mater. **11**, 694 (2012).
[47] V. Kocsis, T. Nakajima, M. Matsuda, A. Kikkawa, Y. Kaneko, J. Takashima, K. Kakurai, T. Arima, Y. Tokunaga, Y. Tokura, and Y. Taguchi, Phys. Rev. B **101**, 075136 (2020).
[48] M. A. Manekar, S. Chaudhary, M. K. Chattopadhyay, K. J. Singh, S. B. Roy, and P. Chaddah, Phys. Rev. B **64**, 104416 (2001).
[49] K. Sengupta and E. V. Sampathkumaran, Phys. Rev. B **73**, 020406(R) (2006).
[50] M. K. Chattopadhyay, M. A. Manekar, A. O. Pecharsky, V. K. Pecharsky, K. A. Gschneidner, Jr., J. Moore, G. K. Perkins, Y. V. Bugoslavsky, S. B. Roy, P. Chaddah, and L. F. Cohen, Phys. Rev. B **70**, 214421 (2004).
[51] A. F. Gubkin, L. S. Wu, S. E. Nikitin, A. V. Suslov, A. Podlesnyak, O. Prokhnenko, K. Prokeš, F. Yokaichiya, L. Keller, and N. V. Baranov, Phys. Rev. B **97**, 134425 (2018).
[52] E. V. Sampathkumaran and A. Niazi, Phys. Rev. B **65**, 180401(R) (2002).
[53] S. Rayaprol, K. Sengupta, and E. V. Sampathkumaran, Phys. Rev. B **67**, 180404(R) (2003).
[54] D. Flahaut, S. Hébert, A. Maignan, V. Hardy, C. Martin, M. Hervieu, M. Costes, B. Raquet, and J. M. Broto, Eur. Phys. J. B **35**, 317 (2003).
[55] N. Mohapatra, K. K. Iyer, S. Rayaprol, and E. V. Sampathkumaran, Phys. Rev. B **75**, 214422 (2007).
[56] V. Hardy, M. R. Lees, A. Maignan, S. Hébert, D. Flahaut, C. Martin, and D. McK Paul, J. Phys.: Condens. Matter **15**, 5737 (2003).
[57] D. Mikhailova, B. Schwarz, A. Senyshyn, A. M. T. Bell, Y. Skourski, H. Ehrenberg, A. A. Tsirlin, S. Agrestini, M. Rotter,

P. Reichel, J. M. Chen, Z. Hu, Z. M. Li, Z. F. Li, and L. H. Tjeng, Phys. Rev. B **86**, 134409 (2012).

[58] W. B. Yelon, D. E. Cox, and M. Eibschütz, Phys. Rev. B **12**, 5007 (1975).

[59] S. Niitaka, H. Kageyama, K. Yoshimura, K. Kosuge, S. Kawano, N. Aso, A. Mitsuda, H. Mitamura, and T. Goto, J. Phys. Soc. Jpn. **70**, 1222 (2001).

[60] S. Niitaka, K. Yoshimura, K. Kosuge, M. Nishi, and K. Kakurai, Phys. Rev. Lett. **87**, 177202 (2001).

[61] J. Singleton, J. W. Kim, C. V. Topping, A. Hansen, E. D. Mun, S. Chikara, I. Lakis, S. Ghannadzadeh, P. Goddard, X. Luo, Y. S. Oh, S. W. Cheong, and V. S. Zapf, Phys. Rev. B **94**, 224408 (2016).

[62] T. Takagi and M. Mekata, J. Phys. Soc. Jpn. **64**, 4609 (1995).